Edge Structures for Nanoscale Graphene Islands on Co(0001) Surfaces

Deborah Prezzi,[†,⊥,¶] Daejin Eom,[‡,§,⊥,¶,△] Kwang T. Rim,[‡] Hui Zhou,[§,▼] Shengxiong Xiao,[‡,□] Colin Nuckolls,[‡] Tony F. Heinz,[§,∥,*] George W. Flynn,[‡,*] and Mark S. Hybertsen[#,*]

[†]Nanoscience Institute, CNR, S3 Center, I-41125 Modena, Italy, [‡]Department of Chemistry, [§]Department of Physics, [⊥]Center for Electron Transport in Molecular Nanostructures, and [∥]Department of Electrical Engineering, Columbia University, New York, New York 10027, United States, and [#]Center for Functional Nanomaterials, Brookhaven National Laboratory, Upton, New York 11973, United States. [¶]Both authors shared equally in the work of this paper. D.P. had major responsibility for the theoretical calculations, and D.E. had major responsibility for the experiments. [△]Present address: Korea Research Institute of Standards & Science, Taejon, South Korea. [▼]Present address: ASML-Brion, 4211 Burton Drive, Santa Clara, CA 95054.

ABSTRACT Low-temperature scanning tunneling microscopy measurements and first-principles calculations are employed to characterize edge structures observed for graphene nanoislands grown on the Co(0001) surface. Images of these nanostructures reveal straight well-ordered edges with zigzag orientation, which are characterized by a distinct peak at low bias in tunneling spectra. Density functional theory based calculations are used to discriminate between candidate edge structures. Several zigzag-oriented edge structures have lower formation energy than armchair-oriented edges. Of these, the lowest formation energy configurations are a zigzag and a Klein edge structure, each with the final carbon atom over the hollow site in the Co(0001) surface. In the absence of hydrogen, the interaction with the Co(0001) substrate plays a key role in stabilizing these edge structures and determines their local conformation and electronic properties. The calculated electronic properties for the low-energy edge structures are consistent with the measured scanning tunneling images.

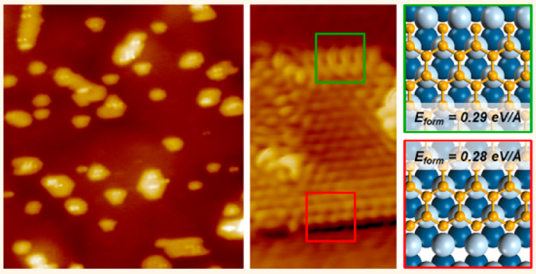

KEYWORDS: graphene · graphene edge structure · graphene on transition metals · graphene growth on transition metals · scanning tunneling microscopy · density functional theory

Edge structure strongly influences the electronic properties of graphene nanostructures,[1,2] stimulating diverse approaches to grow or fabricate such nanostructures with control of the edge morphology.[3,4] Among them, bottom-up techniques have resulted in the fabrication of ultrathin armchair-edged, graphene nanoribbons (GNRs),[5] with electronic properties showing the predicted behavior of ideally controlled structures.[6] Controlled unzipping of carbon nanotubes[7,8] has allowed experimental resolution of edge states of chiral GNRs.[9] Under conditions of electron irradiation, transmission electron microscopy has resolved several edge structures of free-standing graphene, including reconstructions, fascinating dynamics and the role of hydrogen termination.[10−12] Growth of graphene on transition metal substrates from various precursors has also resulted in well-defined edges, which tend to have zigzag orientation.[13−19] In this case, however, evidence is emerging for the importance of strong interaction with the substrate at the graphene edge.[20,21] While the orientation of the edges of graphene nanostructures on transition metal substrates is easily discerned, the detailed atomic structure, including possible reconstructions, has been hard to establish. Transition-metal-catalyzed growth of graphene has emerged as a versatile approach to produce graphene with different characteristics.[22−28] Initial efforts to understand the growth process highlight the key role of edge structure.[29−32] In particular, the interplay between local structure and carbon bonding to the transition metal dictates the local registry and stability.

Nanoscale islands of graphene grown on transition metal substrates with a near lattice match to graphene offer a particularly useful laboratory for further investigation. Particularly good candidate substrates are Ni(111) and Co(0001) with lattice mismatch for graphene of 1.3 and 1.8%, respectively.[33] Figure 1a displays examples of the topography of small, epitaxially grown graphene islands on Co(0001) as determined by scanning tunneling microscopy (STM). As previously

* Address correspondence to tony.heinz@columbia.edu, gwf1@columbia.edu, mhyberts@bnl.gov.

Received for review January 28, 2014 and accepted May 15, 2014.

Published online May 15, 2014
10.1021/nn500583a

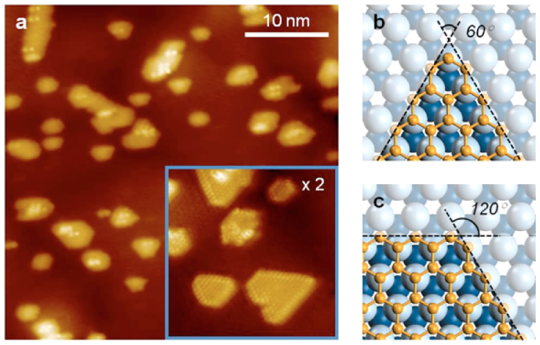

Figure 1. STM topography of graphene islands grown on a Co(0001) surface. (a) Typical 40 × 40 nm^2 image of graphene structures on Co, which was recorded at a temperature of 4.9 K with a $V_{sample} = -0.1$ V and $I_t = 0.5$ nA. The inset shows a zoom over a 10 × 10 nm^2 area (sample bias of −6 mV and tunneling current of 2.0 nA), in which graphene structures with straight well-ordered edges are prevalent. (b,c) Schematic of triangular and hexagonal corners, respectively, for zigzag-edged graphene structures on Co(0001). The carbon atoms are shown in yellow; the topmost and the second layer cobalt atoms are in light and dark blue, respectively.

discussed,[14] these graphene structures exhibit an on-top registry with respect to the substrate: one of two carbon atoms in the graphene unit cell sits directly above the underlying metal atom, while the other carbon atom is located in either a hexagonal close-packed hollow site or a face-centered cubic hollow site of the cobalt substrate. At higher magnification (see inset), we can distinguish graphene islands of different shapes and sizes that exhibit straight ordered edges. A detailed analysis of the registry of C atoms with respect to the clean Co surface reveals that the straight edges have zigzag orientation. The selective formation of such an edge conformation, which is not the most stable for isolated or weakly interacting systems,[34−36] points to the crucial role played by the TM substrate which is able to drive the growth along a preferential direction.

Several points follow strictly from geometric constraints. With fixed edge chirality, commensurate graphene can form islands with either 60 or 120° angles at their corners. In the first case, the peripheral atoms maintain the same registry (zigzag edge atoms are always in the on-top or hollow sites, Figure 1b). In the second case, adjacent edges display two opposite configurations (Figure 1c). Furthermore, opposite sides of a hexagonal-shaped island must also have opposite registry. In practice, while the lattice mismatch between graphene and Co(0001) is finite, this analysis applies to islands that are sufficiently small, here typically a few nanometers in extent. (The simplest measure of a commensurability length scale gives about 14 nm for the 1.8% lattice mismatch for Co(0001). A more complex analysis, including the trade off between energy gain for a commensurate region and defect formation energy in the graphene, is beyond the scope of this work.) In order to understand the observed island structures, the formation energy and the geometry of the local reconstruction of both registries for the zigzag edges will be essential.

In this work, we use low-temperature scanning tunneling microscopy and first-principles calculations to study the structure and electronic properties of the edges of graphene islands grown on the Co(0001) surface. Calculations reveal that interaction with the substrate selectively stabilizes an unreconstructed zigzag and Klein edge structure, each with the final C atom over the hollow site on the surface and with similar formation energies. In the STM images, these two edges have a different height profile and a different electronic contrast. The stability of the Klein edge structure is essential to explain the appearance of all six possible zigzag-oriented edges on nanometer-scale islands with essentially equal probability. The two different edges are distinguishable in STM images.

RESULTS AND DISCUSSION

Following the analysis in Figure 1, the first fundamental evidence characterizing the on-top *versus* hollow terminated zigzag edges is the relative rate at which they occur across a series of islands. In order to quantify this, we have analyzed several STM images on the basis of island corner angles (see Figure 2). As shown in Figure 2a, we decorated the edge boundaries of graphene islands with two different colors (*i.e.*, red and yellow) such that two different colors meet each other at the corner angle of 120 or 240°, and the same colors meet at the corner angle of 60 or 300°. For each island, we calculated the ratio between the total length of red and yellow segments; the histogram of the red-to-yellow ratio distribution is displayed in Figure 2b. (Note that we assumed that the nearly horizontal bottom edge of each island has the same edge type. Then, two different colors represent two different edge types within each island, although the same colors for two different islands do not necessarily represent the same edge type. Note also that only islands having closed shapes within the image frame of Figure 2a were considered in the counting.) The histogram plot clearly shows that the majority of the islands have a red-to-yellow ratio close to the unity (median = 0.91; 71% of the islands are within 30% of the median). The island perimeters range from 5 to 25 nm with no correlation between edge ratio and perimeter. The edge distribution resulting from this analysis indicates a nearly equal presence for the two edge configurations. This implies that both sites (*i.e.*, on-top site and hollow site) form with basically equal probability during the growth of the graphene islands on Co(0001).

To investigate the electronic structure, the edge region of several islands was locally probed by STM and compared to the interior region. Two examples of such scanning tunneling spectroscopy (STS) are shown

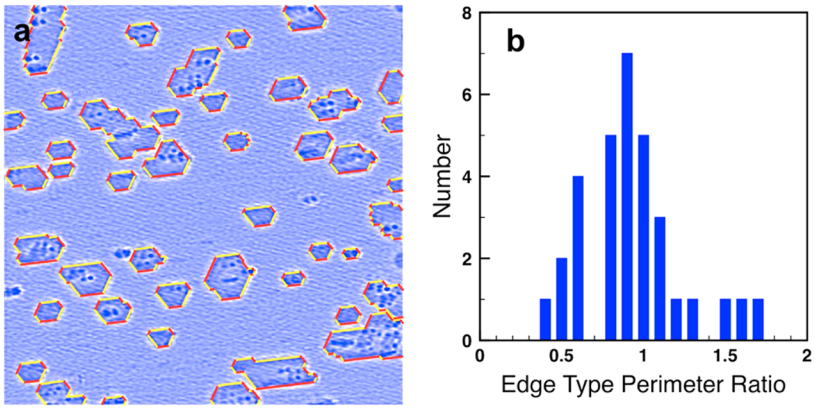

Figure 2. Statistical analysis of graphene edge distribution. (a) STM topography of several graphene islands on the Co(0001) surface, which is imaged at 4.9 K with $V_{sample} = -0.1$ V and $I_t = 0.5$ nA. The image size is 40 × 40 nm^2. A different color scale is used to highlight the edge locations, which are further emphasized by overlaying red or yellow lines. For each island in (a), the ratio between the total length of red segments and that of yellow segments is calculated. (b) Histogram plot of the calculated edge type perimeter ratios from (a).

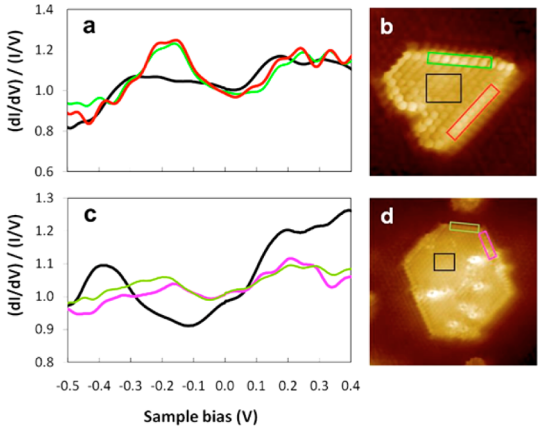

Figure 3. Normalized conductance curves, (d*I*/d*V*)/(*I*/*V*), from STS measurements comparing different edge regions to the body of the islands. Data for a representative triangular island (a,b) and hexagonal island (c,d) on the Co(0001) surface are shown. Normalized conductance spectra are shown in (a) and (c). These are averaged over the rectangular regions outlined in the topographic images shown in (b) and (d), following the color scheme adopted for the boxes. The topographs are imaged at 4.9 K, with $V_{sample} = -3$ mV and $I_t = 2$ nA. The image sizes are 5 × 5 and 10 × 10 nm^2 for triangular and hexagonal islands, respectively.

in Figure 3. The normalized conductance curves are averaged over rectangular regions shown on the corresponding topographic image, two near the edges and one in the middle of each island. We see that, unlike the interior region, the spectral response near the edges exhibits a peak centered at −0.18 eV below the Fermi level (E_F). Another feature, beginning near +0.1 to 0.2 eV and possessing rather a broad energy distribution, is also noticeable in the spectra of Figure 3. However, that feature is common to both the edge and the interior regions of the island, so it is unlikely to be an edge-specific response. At about the same energy, similar features are observed while scanning the edge region of several islands. In particular, we observe no significant differences for curves arising from adjacent edges of hexagonal islands, despite the fact that they would nominally have a different configuration (*i.e.*, on-top *vs* hollow).

To gain further insight into the stability and morphological details as well as the electronic structure of graphene edges in the presence of the Co(0001) substrate, we have employed first-principles density functional theory (DFT) simulations. The formation energy of the edges has been probed by considering several prototype systems. These consist of graphene stripes of nanometric width (*i.e.*, graphene nanoribbons), as well as triangular graphene nanostructures of similar sizes (see Supporting Information, Figures S1 and S2). For substrates with near lattice matching to the graphene, opposite edges in armchair graphene nanoribbons are the same. However, zigzag graphene nanoribbons always exhibit topologically distinct edges; that is, opposite edges have different registry (hollow *vs* on-top) with respect to the Co(0001) substrate. Distinguishing the formation energy of these two distinct edges is one of our primary objectives. Therefore, we also considered several nanometer-scale triangular nanostructures terminated with zigzag peripheral atoms having all the same registry to the underlying Co lattice, as shown in Figure S2. In this way, the aggregate data can be used to disentangle the separate formation energy of different edge configurations. To achieve this, we further assume that the formation energy can be modeled as a local property, that is, as the sum of independent edge atom formation energies. When the data are analyzed in this way, the solution for the separate edge formation energies meets all the constraints within 0.03 eV/Å.

Comparing the formation energies for hydrogen-passivated zigzag and armchair edge configurations (0.2 eV/Å *versus* 0.3 eV/Å, further details in Table S1), the zigzag edge is indeed found to be more stable than the armchair one upon adsorption on Co, irrespective

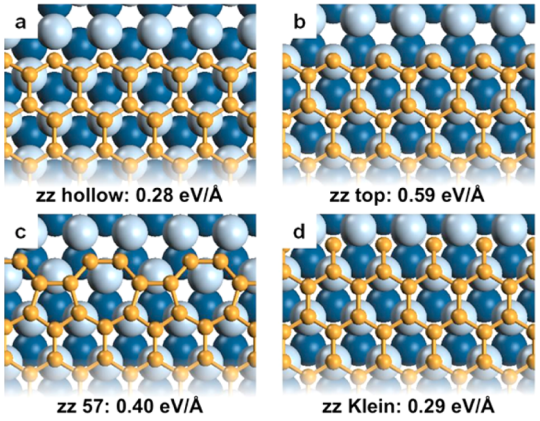

Figure 4. Ball-and-stick models for different edge conformations along the zigzag direction. Clean zigzag edges can place the terminal C atom in hollow (a) or on-top (b) positions. Each of these can be further modified to form distinct edge morphologies, such as a 57-reconstructed edge (c) or a Klein termination (d). Carbon atoms are depicted in yellow; the topmost and the second layer cobalt atoms are in light and dark blue, respectively.

of the zigzag edge registry with respect to the substrate (*i.e.*, on-top or hollow). However, under the growth conditions used in the experiments, the temperature substantially exceeds that for hydrocarbon dehydrogenation and H_2 desorption (about 410 K) on Co(0001).[37] The edges are thus expected to be unpassivated. In this case, we find instead that the registry of the terminal C atom is a critical factor in determining the stability: the zigzag hollow edge (Figure 4a) is significantly more stable (0.28 eV/Å) than the on-top one (Figure 4b, 0.59 eV/Å), and the armchair edge has a formation energy between these two (0.49 eV/Å), when constrained to the on-top geometry. (Upon full geometrical optimization, the structure spontaneously relaxes to bridge position, with a formation energy of 0.43 eV/Å.) These results agree with previous calculations,[30−32] although only the average zigzag formation energy has been calculated previously. For the first time, we now see that there is a substantial difference in this energy depending on registry (on-top *versus* hollow).

From this analysis and under the experimental conditions mentioned above, we would thus expect the formation of clean zigzag-terminated triangular islands with edge atoms always over the hollow site. This clearly contrasts with experimental observations and motivated consideration of a number of possible modifications of the on-top registered zigzag edge which could lower its formation energy: a 57-reconstruction[38] (Figure 4c), a Klein termination[39] (Figure 4d), and a reconstruction of the Klein termination where the terminal C atoms pair to form five-fold rings at the edge.[40] From our results, the Klein termination emerges as the most stable one for the top edge, with a formation energy similar to that of the zigzag hollow site. It is also worth noting that these two lowest formation energy edges cost only a few tens of meV/Å more to form than passivated zigzag edges, indicating that a considerable energy gain comes from the edge−substrate interaction. As to the 57-reconstruction, it indeed lowers the top edge energy substantially. Although this is not the favored edge thermodynamically, this reconstruction is more likely to form than the armchair termination. Finally, the Klein reconstruction, with five-fold rings at the edge, is not stable, relaxing back to the pure Klein configuration. This highlights the strong C−Co interaction at this edge. The stabilization of the Klein edge seen here is analogous to recently discussed armchair-adatom edge structures,[30,31] although the calculated reduction in edge formation energy for Co(0001), upon addition of the adatom, is smaller than what we find for the present Klein case. Also, a recent calculation for the Klein reconstruction on Co(0001), termed the zigzag-adatom edge in that work, showed a substantially higher formation energy due to a different registration of the edge relative to the surface Co atoms.[30]

In summary, the DFT-calculated formation energies suggest that, for a hexagonal island with 120° corners, the alternating edges will be zigzag hollow and Klein structures. For triangular islands, the edges can be either zigzag hollow or Klein structures, but not a mixture. Furthermore, these low-energy edges have similar formation energies on Co(0001), consistent with the observation from the STM images that they occur in as-grown islands with roughly equal probability.

A key question is the degree to which these distinct edge structures are distinguishable in the STM images. Figure 5a displays a portion of the topography of an elongated island characterized by parallel edges separated by a nondefective central region (see Figure S4 for the full island image). This allows us to define the registry (parallel gray dashed lines) across the edges, which have opposite configurations by construction. For edge type A (bottom edge), the features of the brightest intensity (*i.e.*, yellow dashed line) exhibit a spherical ball shape. On the other hand, features of edge type B (upper edge) display an elongated feature shape and also fall off registry (*i.e.*, between the yellow dashed lines). A similar, qualitative distinction between two, straight edge morphologies can be made in high-resolution images of other islands, as well, including a triangular example in which only one type of edge is observed (Figure S5). The simulated low-bias STM image based on the calculated graphene nanoribbon structure with Klein edge at the top and zigzag hollow edge at the bottom (shown in Figure 5b, −0.05 eV) similarly shows a distinguishable shape in the bright, near-edge localized features. The zigzag hollow edge is relatively bright, with a zigzag pattern encompassing the third and fourth rows. The Klein edge exhibits bright features that are more oval-shaped and appear over the bond between the third and fourth rows. The

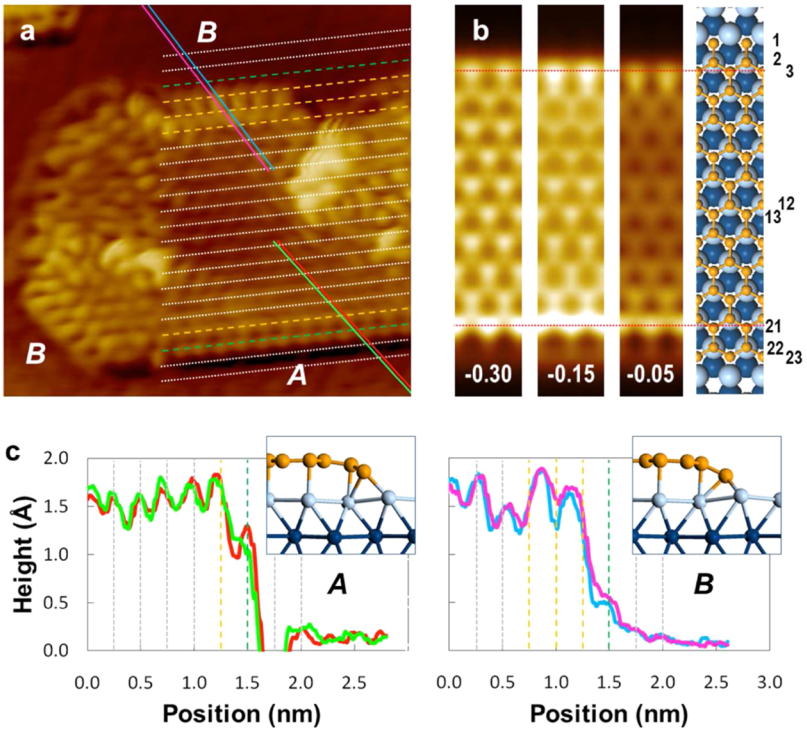

Figure 5. Height profiles across edge regions. (a) STM topographic image of a graphene island on the Co(0001) surface, taken at 4.9 K with $V_{sample} = -0.02$ V and $I_t = 2$ nA. The image size is 5 × 5 nm^2. The dotted and dashed lines are overlaid to highlight a series of atomic rows with 2.5 Å spacing. (b) Simulated constant current images for bias windows of 0.30, −0.15, and −0.05 eV, based on DFT calculations for a ribbon with a Klein termination (top) and a hollow termination (bottom). The adjacent ball-and-stick structure provides a scaled and aligned guide to the underlying atomic structure. (c) Height profiles taken along four solid lines that cross the edges, following the color scheme in (a). The vertical dotted or dashed lines indicate the position of the guide line with the same line style and color code adopted in (a). Insets show the calculated atomic structure near each edge in side view.

simulated image also highlights the fact that the last two rows of C atoms are suppressed in the topographic images. Indeed, the significant distortion of the structure at the edge induced by the strong C−Co interaction reduces the effective width of the ribbon, thereby moving the edge-localized features a few rows in with respect to the physical width.

Figure 5c shows STM line profiles taken across the edges at low negative bias (−0.02 V and 2 nA). As can be clearly seen, the A and B edges show rather different features in the height profile, as well. For both edges, there are additional weak features, outside the last prominent feature, that differ in apparent height. For comparison, the side view of the simulated edge structure also shows a clear difference in height profile (insets in Figure 5c). The substantial distortion of the nanoribbon edge caused by the terminal C atom being positioned so as to form a strong bond with a surface Co atom shows a different magnitude for the height change (0.6 and 0.8 Å for hollow and Klein, respectively). The magnitude of that distortion corresponds well with the apparent height in the measured line scans. Taken together, all of this suggests that the A edges are of zigzag hollow type and the B edges are unreconstructed Klein edges.

Returning to Figure 3, we still need to understand why two such apparently different physical edge structures might give very similar electronic features, as seen in the tunneling spectroscopy measurements. To probe this question, we analyze the projected density of states from the DFT calculations in order to identify candidate states that can contribute to the STS; details are discussed under Methods. Results are shown in Figure 6 for selected rows across the graphene nanoribbon structure studied in Figure 5b. The top panel illustrates the fact that, at negative bias, the electronic signature for graphene commensurate with Co(0001) consists of a main peak and a low-energy shoulder in the range from 0 to −0.4 eV. This complex corresponds to the spin up p_z state on the C atom over the hollow site on the surface strongly coupled to Co d states.[14] The low-energy shoulder corresponds to states near the K point in the surface Brillouin zone, while the main peak reflects the increasing interaction with the Co d states that leads to reduced dispersion further form the K point and the PDOS peak near −0.4 eV. This feature is replicated near the center of the graphene nanoribbon (row 13). While moving toward the edges, the shoulder resolves into a peak that appears for both edge types at about −0.10 to −0.15 eV (see arrows). This edge feature is related to the first nondistorted graphene-like hollow site C atom. Furthermore, this peak plays a key role in the bright, near-edge feature visible on both sides of the simulated STM images in Figure 5b. This all suggests that

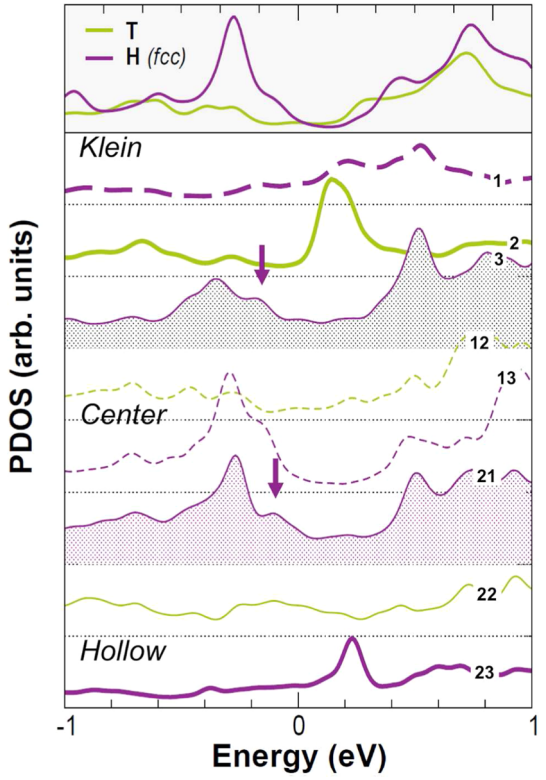

Figure 6. Calculated projected density of states (PDOS) on the C atomic p_z orbital for selected atomic rows from the nanoribbon structure illustrated in Figure 4. The top panel shows the same calculation for the two distinct sites (on-top, T, green; hollow, H, purple) for commensurate monolayer graphene on a Co(0001) structure. Rows 3 and 21 correspond to the bright, near-edge features in the simulated topographic images in Figure 4. The calculated PDOS for these rows are highlighted by shading below the curves and exhibit a shoulder near −0.15 to −0.20 eV indicated by the arrows.

the similar STS features observed at negative bias for different edges can be related to the same type of atom, that is, the first, undistorted C atom over the hollow site. The details of the bright features in the simulated images are bias-dependent (see Figure 5b and Figure S3). In particular, there is a clear increase in the intensity near the edges of the simulated images for a bias window of −0.15 eV relative to that for both −0.30 and −0.05 eV. All together, this is consistent with the peak near −0.2 V in the measured STS near the edges of the islands. Interestingly, the calculations also suggest empty edge states in the 0.2−0.5 eV range (see Figure 6 and the simulated STM image in Figure S3). While the STS in Figure 3 clearly indicates features in this voltage range, the STS data for the edges have similar strength to that in the center of the islands and they do not appear to depend in any substantial way on which edge is probed.

Another interesting factor may be the finite size and shape of the islands observed in this study. For a free-standing island, there is a fundamental difference between triangular and hexagonal cases: the former has an imbalance in the number of sites of one sublattice *versus* the other. This has direct implications for the magnetic properties, and the relative number of edge-localized states in the hexagonal case is lower.[41] For graphene on Co(0001), however, a strong electronic coupling between the C sublattice that is on-top of the Co atoms breaks the sublattice symmetry. This, together with the two distinct edge structures and strong interactions between the edge atoms and the Co substrate, raises the question as to the extent to which the bright, near-edge localized features in the images display any remnant of the spin polarization expected for ideal zigzag edges.[1,42] Analysis of the spin polarization in the DFT calculations (Figure 7) clearly shows that the edge spin polarization is largely quenched, in agreement with recent calculations for passivated zigzag nanoribbons on Ni(111).[43] However, this does not exclude more subtle boundary and interference effects for the frontier electronic states that are primarily responsible for the STM images. Interestingly, for sufficiently small triangular islands, such effects emerge in the measured topographic images (Figure S6). In simulated images for small triangular islands, the pattern of bright features clearly changes with bias window and depends on the edge termination (zigzag *versus* Klein, Figure S7). In view of this, the differences in features seen in STS in Figure 3 above between a roughly triangular and a hexagonal island, both in the center and at the edges, may not be surprising.

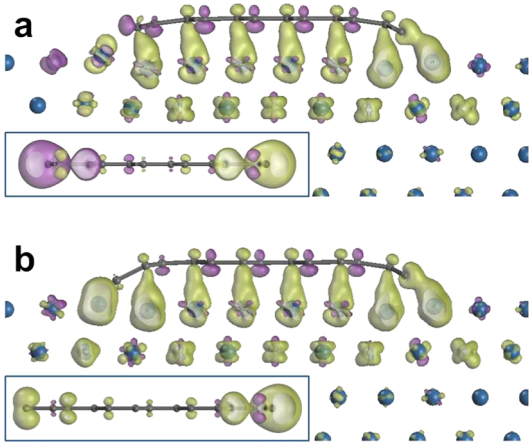

Figure 7. Spin polarization of zigzag GNRs on Co(0001). (a) Spin polarization for a GNR characterized by zigzag top (left) and hollow (right) clean edges. (b) Spin polarization for a GNR characterized by Klein top (left) and clean hollow (right) edges. The spin polarization of the Co slab has been subtracted from the total polarization to highlight the effect produced on GNRs. The spin polarization of the corresponding isolated GNRs is shown (insets) for comparison. All plots are displayed for the same isosurface value of ±0.004 *e*/au,[3] where the two spin channels are shown in violet and green.

CONCLUSIONS

STM studies of graphene islands formed on the Co(0001) surface show regular, relatively straight

zigzag-oriented edges. Analysis of the images indicates that two topologically distinct edge structures form with essentially equal probability. The conditions of the experiment suggest that the edges are not passivated by H. In order to apply atomic-scale models to understand the occurrence of both edges, a scheme was developed, based on DFT calculations for several structures, to disentangle the formation energy of the two distinct edges for the first time. The study reveals that the unpassivated zigzag edge with the final C atom over the surface hollow site has the lowest formation energy. For the topologically distinct edge, the calculations show that a Klein edge structure with the singly coordinated terminal C atom over a surface hollow site has a formation energy that is only slightly higher. This stands in stark contrast to the energetics for free-standing graphene edges. The nominally unpassivated edges interact strongly with the Co surface, passivating the dangling bonds and significantly affecting the edge electronic properties. In particular, analysis of the measured STM images and the simulated STM images suggests that the last two rows of C atoms are suppressed in the images due to that strong interaction. Furthermore, the images of the edges on opposite sides of islands that should be topologically distinct are consistent with the difference predicted for the zigzag edge and the Klein edge.

Ongoing efforts to develop atomic-scale models for graphene growth on transition metal surfaces naturally hinge on the relative stability of different edge structures.[29−32] In particular, the role of singly coordinated C atoms at the edge has already been considered in this context. Our results show that such an edge structure, the Klein edge discussed here, can have relatively low formation energy and likely plays a key role in the observation of hexagonal graphene islands on Co(0001) surfaces.

METHODS

The experiments were performed using a low-temperature scanning tunneling microscope (STM) in an ultrahigh vacuum (UHV) chamber at a base pressure was 3×10^{-11} Torr. The structural and electronic properties of the samples were measured by the STM at a temperature of 4.9 K. The samples were prepared starting with a cobalt single crystal with (0001) orientation that was cleaned *in situ* by repeated cycles of argon-ion sputtering and subsequent thermal annealing at 570 K. Contorted hexabenzocoronene (HBC) molecules[44] were deposited by vacuum evaporation from a source at 605 K onto this cobalt basal plane while it was held at 300 K. The cobalt substrate and adsorbed HBC molecules were then annealed *in situ* for 20 min at a temperature of 600 K, which is well above the dehydrogenation and H_2 desorption temperature (∼410 K) for hydrocarbons on Co(0001).[37] This procedure resulted in the growth of nanometer-scale graphene islands on Co(0001), as we have described previously.[14]

DFT calculations were performed using plane waves and ultrasoft pseudopotentials, as implemented in the Quantum ESPRESSO package.[45] The plane wave kinetic energy cutoff for the wave functions (charge density) was set to 25 (300) Ry. We used the following pseudopotentials: Co.pz-nd-rrkjus.UPF, C.pz-van_ak.UPF, and H.pz-rrkjus.UPF, as taken from the webpage of the code http://www.quantum-espresso.org/. The local spin density approximation (LSDA) was employed, according to the Perdew−Zunger parametrization (LSDA).[46,47]

The initial configuration of each structure (Figures S2 and S3) was chosen to have on-top registry with respect to the substrate, that is, the lowest energy geometry found for the full monolayer graphene:Co(0001) interface.[14] The simulation supercells were built from the orthorhombic unit cell of Co(0001), with four planes of Co and a 1×6 (8×1) lateral periodicity to accommodate zigzag (armchair) GNRs. The in-plane lattice parameter was set equal to 2.42 Å, the optimized parameter for bulk Co.[14] The lattice mismatch with graphene calculated in LSDA is close in magnitude to that from experiment.[33] Slab replicas were separated by a vacuum region of 9 Å. A 36×4 (5×20) *k*-point sampling was employed for summations over the BZ in the zigzag (armchair) case. Triangular graphene nanostructures with (zigzag) edge length of about 1.24 nm were simulated in 9×9 hexagonal supercells, using a 4×4 *k*-point sampling. The atomic positions within the cell were fully relaxed, with a force threshold of 10^{-4} au.

For each relaxed graphene nanostructure (GNS), the zero-temperature edge formation energy per length is computed as

$$\varepsilon_{edge}(T = 0K) = [E_{tot}(GNS:Co) + E_{ZPE} - N_{Co}\mu(Co) + -N_C\mu(C) - N_H\mu(H:Co) - N_C E_{ads}(MG:Co)]/2L$$

where E_{tot}(GNS:Co) is the total energy of the GNS:Co slab; E_{ZPE} is the zero-point energy due to C−H bonds; μ(Co), μ(C), and μ(H:Co) are the chemical potentials of Co in the slab, of C in isolated graphene, and of H adsorbed on the Co(0001) surface, respectively. To single out the edge formation energy, we also subtract the adsorption energy per C atom obtained for the monolayer graphene/Co interface E_{ads}(MG:Co).

The projected density of states, for each inequivalent C atom across the GNR width, is calculated by summing the projections of each state onto reference atomic p_z orbitals of C, for both minority and majority spin channels. The use of LSDA energy levels to interpret the peaks in the STS comes with the caveat that there may be corrections to the peak positions. Based on the GW approach to electronic excitations, there can be substantial corrections to the energy levels of molecules weakly interacting with a metal support.[48,49] For graphene nanostructures, similarly weakly interacting with a metal support, corrections for the effect of the image potential can be included.[6,50] However, in the present scenario, the graphene nanostructures have stronger electronic interaction with the metal and simple models for the corrections to LSDA orbital energies no longer apply.[51] Detailed calculations with the GW approach for the present model structures are complex and beyond the scope of the present work.

Conflict of Interest: The authors declare no competing financial interest.

Acknowledgment. We thank M. Lefenfeld for contributions to the early phases of the experiments reported here. This work was supported by the U.S. Department of Energy (DE-FG02-88-ER13937 to G.W.F., DE-FG02-07ER15842 to T.F.H., and DE-AC02-98CH10886 to M.S.H.), by the National Science Foundation through the NSEC Program (CHE-06-41523), by the New York State Office of Science, Technology, and Academic Research (NYSTAR), by the Air Force Office of Scientific Research (MURI FA955009-1-0705), and by the Italian Ministry of Research (Grant No. PRIN-20105ZZTSE to D.P.). Research was conducted in part with facilities of CINECA and in part with facilities of the Center for Functional Nanomaterials at Brookhaven National Laboratory, supported by the U.S. Department of Energy, Office of Basic Energy Sciences, under contract number

DE-AC02-98CH10886. Equipment and material support was provided by the National Science Foundation through Grant CHE-10-12058 (to G.W.F.).

Supporting Information Available: Details of the graphene nanostructures considered with the DFT calculations, including images of the structures and details of the simulation cells. Details of the calculated edge formation energies. Bias dependence of the simulated STM images for the structure shown in Figure 5b. Additional STM images and simulated STM images for triangular nanostructures. This material is available free of charge *via* the Internet at http://pubs.acs.org.

REFERENCES AND NOTES

1. Nakada, K.; Fujita, M.; Dresselhaus, G.; Dresselhaus, M. S. Edge State in Graphene Ribbons: Nanometer Size Effect and Edge Shape Dependence. *Phys. Rev. B* **1996**, *54*, 17954.
2. Ritter, K. A.; Lyding, J. W. The Influence of Edge Structure on the Electronic Properties of Graphene Quantum Dots and Nanoribbons. *Nat. Mater.* **2009**, *8*, 235–242.
3. Jia, X. T.; Campos-Delgado, J.; Terrones, M.; Meunier, V.; Dresselhaus, M. S. Graphene Edges: A Review of Their Fabrication and Characterization. *Nanoscale* **2011**, *3*, 86–95.
4. Zhang, X.; Xin, J.; Ding, F. The Edges of Graphene. *Nanoscale* **2013**, *5*, 2556–2569.
5. Cai, J.; Ruffieux, P.; Jaafar, R.; Bieri, M.; Braun, T.; Blankenburg, S.; Muoth, M.; Seitsonen, A. P.; Saleh, M.; Feng, X.; *et al.* Atomically Precise Bottom-up Fabrication of Graphene Nanoribbons. *Nature* **2010**, *466*, 470–473.
6. Ruffieux, P.; Cai, J.; Plumb, N. C.; Patthey, L.; Prezzi, D.; Ferretti, A.; Molinari, E.; Feng, X.; Müllen, K.; Pignedoli, C. A.; *et al.* Electronic Structure of Atomically Precise Graphene Nanoribbons. *ACS Nano* **2012**, *6*, 6930–6935.
7. Kosynkin, D. V.; Higginbotham, A. L.; Sinitskii, A.; Lomeda, J. R.; Dimiev, A.; Price, B. K.; Tour, J. M. Longitudinal Unzipping of Carbon Nanotubes To Form Graphene Nanoribbons. *Nature* **2009**, *458*, 872–876.
8. Jiao, L.; Zhang, L.; Wang, X.; Diankov, G.; Dai, H. Narrow Graphene Nanoribbons from Carbon Nanotubes. *Nature* **2009**, *458*, 877–880.
9. Tao, C.; Jiao, L.; Yazyev, O. V.; Chen, Y.-C.; Feng, J.; Zhang, X.; Capaz, R. B.; Tour, J. M.; Zettl, A.; Louie, S. G.; *et al.* Spatially Resolving Edge States of Chiral Graphene Nanoribbons. *Nat. Phys.* **2011**, *7*, 616–620.
10. Girit, C. O.; Meyer, J. C.; Erni, R.; Rossell, M. D.; Kisielowski, C.; Yang, L.; Park, C.-H.; Crommie, M. F.; Cohen, M. L.; Louie, S. G.; *et al.* Graphene at the Edge: Stability and Dynamics. *Science* **2009**, *323*, 1705–1708.
11. Kim, K.; Coh, S.; Kisielowski, C.; Crommie, M. F.; Louie, S. G.; Cohen, M. L.; Zettl, A. Atomically Perfect Torn Graphene Edges and Their Reversible Reconstruction. *Nat. Commun.* **2013**, *4*, 2723.
12. He, K.; Lee, G.-D.; Robertson, A. W.; Yoon, E.; Warner, J. H. Hydrogen-Free Graphene Edges. *Nat. Commun.* **2014**, *5*, 3040.
13. Coraux, J.; N'Diaye, A. T.; Engler, M.; Busse, C.; Wall, D.; Buckanie, N.; Heringdorf, F.; van Gastei, R.; Poelsema, B.; Michely, T. Growth of Graphene on Ir(111). *New J. Phys.* **2009**, *11*, 22.
14. Eom, D.; Prezzi, D.; Rim, K. T.; Zhou, H.; Lefenfeld, M.; Xiao, S.; Nuckolls, C.; Hybertsen, M. S.; Heinz, T. F.; Flynn, G. W. Structure and Electronic Properties of Graphene Nanoislands on Co(0001). *Nano Lett.* **2009**, *9*, 2844–2848.
15. Tian, J.; Cao, H.; Wu, W.; Yu, Q.; Chen, Y. P. Direct Imaging of Graphene Edges: Atomic Structure and Electronic Scattering. *Nano Lett.* **2011**, *11*, 3663–3668.
16. Lu, J.; Yeo, P. S. E.; Gan, C. K.; Wu, P.; Loh, K. P. Transforming C60 Molecules into Graphene Quantum Dots. *Nat. Nanotechnol.* **2011**, *6*, 247–252.
17. Phark, S.-h.; Borme, J.; Vanegas, A. L.; Corbetta, M.; Sander, D.; Kirschner, J. Direct Observation of Electron Confinement in Epitaxial Graphene Nanoislands. *ACS Nano* **2011**, *5*, 8162–8166.
18. Olle, M.; Ceballos, G.; Serrate, D.; Gambardella, P. Yield and Shape Selection of Graphene Nanoislands Grown on Ni(111). *Nano Lett.* **2012**, *12*, 4431–4436.
19. Pan, M.; Girão, E. C.; Jia, X.; Bhaviripudi, S.; Li, Q.; Kong, J.; Meunier, V.; Dresselhaus, M. S. Topographic and Spectroscopic Characterization of Electronic Edge States in CVD Grown Graphene Nanoribbons. *Nano Lett.* **2012**, *12*, 1928–1933.
20. Lacovig, P.; Pozzo, M.; Alfe, D.; Vilmercati, P.; Baraldi, A.; Lizzit, S. Growth of Dome-Shaped Carbon Nanoislands on Ir(111): The Intermediate between Carbidic Clusters and Quasi-Free-Standing Graphene. *Phys. Rev. Lett.* **2009**, *103*, 166101.
21. Cui, Y.; Fu, Q.; Zhang, H.; Bao, X. Formation of Identical-Size Graphene Nanoclusters on Ru(0001). *Chem. Commun.* **2011**, *47*, 1470–1472.
22. Sutter, P. W.; Flege, J.-I.; Sutter, E. A. Epitaxial Graphene on Ruthenium. *Nat. Mater.* **2008**, *7*, 406–411.
23. Kim, K. S.; Zhao, Y.; Jang, H.; Lee, S. Y.; Kim, J. M.; Kim, K. S.; Ahn, J.-H.; Kim, P.; Choi, J.-Y.; Hong, B. H. Large-Scale Pattern Growth of Graphene Films for Stretchable Transparent Electrodes. *Nature* **2009**, *457*, 706–710.
24. Li, X.; Cai, W.; An, J.; Kim, S.; Nah, J.; Yang, D.; Piner, R.; Velamakanni, A.; Jung, I.; Tutuc, E.; *et al.* Large-Area Synthesis of High-Quality and Uniform Graphene Films on Copper Foils. *Science* **2009**, *324*, 1312–1314.
25. Reina, A.; Jia, X.; Ho, J.; Nezich, D.; Son, H.; Bulovic, V.; Dresselhaus, M. S.; Kong, J. Large Area, Few-Layer Graphene Films on Arbitrary Substrates by Chemical Vapor Deposition. *Nano Lett.* **2009**, *9*, 30–35.
26. Gao, L.; Guest, J. R.; Guisinger, N. P. Epitaxial Graphene on Cu(111). *Nano Lett.* **2010**, *10*, 3512–3516.
27. Zhao, L.; He, R.; Rim, K. T.; Schiros, T.; Kim, K. S.; Zhou, H.; Gutiérrez, C.; Chockalingam, S. P.; Arguello, C. J.; Pálová, L.; *et al.* Visualizing Individual Nitrogen Dopants in Monolayer Graphene. *Science* **2011**, *333*, 999–1003.
28. Ago, H.; Ogawa, Y.; Tsuji, M.; Mizuno, S.; Hibino, H. Catalytic Growth of Graphene: Toward Large-Area Single-Crystalline Graphene. *J. Phys. Chem. Lett.* **2012**, *3*, 2228–2236.
29. Luo, Z.; Kim, S.; Kawamoto, N.; Rappe, A. M.; Johnson, A. T. C. Growth Mechanism of Hexagonal-Shape Graphene Flakes with Zigzag Edges. *ACS Nano* **2011**, *5*, 9154–9160.
30. Gao, J.; Zhao, J.; Ding, F. Transition Metal Surface Passivation Induced Graphene Edge Reconstruction. *J. Am. Chem. Soc.* **2012**, *134*, 6204–6209.
31. Artyukhov, V. I.; Liu, Y.; Yakobson, B. I. Equilibrium at the Edge and Atomistic Mechanisms of Graphene Growth. *Proc. Natl. Acad. Sci. U.S.A.* **2012**, *109*, 15136–15140.
32. Shu, H.; Chen, X.; Tao, X.; Ding, F. Edge Structural Stability and Kinetics of Graphene Chemical Vapor Deposition Growth. *ACS Nano* **2012**, *6*, 3243–3250.
33. Karpan, V. M.; Giovannetti, G.; Khomyakov, P. A.; Talanana, M.; Starikov, A. A.; Zwierzycki, M.; van den Brink, J.; Brocks, G.; Kelly, P. J. Graphite and Graphene as Perfect Spin Filters. *Phys. Rev. Lett.* **2007**, *99*, 176602.
34. Okada, S. Energetics of Nanoscale Graphene Ribbons: Edge Geometries and Electronic Structures. *Phys. Rev. B* **2008**, *77*, 041408-4.
35. Wassmann, T.; Seitsonen, A. P.; Saitta, A. M.; Lazzeri, M.; Mauri, F. Structure, Stability, Edge States, and Aromaticity of Graphene Ribbons. *Phys. Rev. Lett.* **2008**, *101*, 096402-4.
36. Gan, C. K.; Srolovitz, D. J. First-Principles Study of Graphene Edge Properties and Flake Shapes. *Phys. Rev. B* **2010**, *81*, 125445.
37. Vaari, J.; Lahtinen, J.; Hautojarvi, P. The Adsorption and Decomposition of Acetylene on Clean and K-Covered Co(0001). *Catal. Lett.* **1997**, *44*, 43–49.
38. Koskinen, P.; Malola, S.; Hakkinen, H. Self-Passivating Edge Reconstructions of Graphene. *Phys. Rev. Lett.* **2008**, *101*, 115502.
39. Klein, D. J. Graphitic Polymer Strips with Edge States. *Chem. Phys. Lett.* **1994**, *217*, 261–265.
40. Ivanovskaya, V. V.; Zobelli, A.; Wagner, P.; Heggie, M. I.; Briddon, P. R.; Rayson, M. J.; Ewels, C. P. Low-Energy Termination of Graphene Edges *via* the Formation of Narrow Nanotubes. *Phys. Rev. Lett.* **2011**, *107*, 065502.
41. Fernandez-Rossier, J.; Palacios, J. J. Magnetism in Graphene Nanoislands. *Phys. Rev. Lett.* **2007**, *99*, 177204-4.

42. Son, Y.-W.; Cohen, M. L.; Louie, S. G. Energy Gaps in Graphene Nanoribbons. *Phys. Rev. Lett.* **2006**, *97*, 216803.
43. Sawada, K.; Ishii, F.; Saito, M. Magnetism in Graphene Nanoribbons on Ni(111): First-Principles Density Functional Study. *Phys. Rev. B* **2010**, *82*, 245426.
44. Xiao, S.; Myers, M.; Miao, Q.; Sanaur, S.; Pang, K.; Steigerwald, M. L.; Nuckolls, C. Molecular Wires from Contorted Aromatic Compounds. *Angew. Chem., Int. Ed.* **2005**, *44*, 7390–7394.
45. Giannozzi, P.; Baroni, S.; Bonini, N.; Calandra, M.; Car, R.; Cavazzoni, C.; Ceresoli, D.; Chiarotti, G. L.; Cococcioni, M.; Dabo, I.; *et al.* Quantum Espresso: A Modular and Open-Source Software Project for Quantum Simulations of Materials. *J. Phys.: Condens. Matter* **2009**, *21*, 395502.
46. Ceperley, D. M.; Alder, B. J. Ground State of the Electron Gas by a Stochastic Method. *Phys. Rev. Lett.* **1980**, *45*, 566.
47. Perdew, J. P.; Zunger, A. Self-Interaction Correction to Density-Functional Approximations for Many-Electron Systems. *Phys. Rev. B* **1981**, *23*, 5048.
48. Neaton, J. B.; Hybertsen, M. S.; Louie, S. G. Renormalization of Molecular Electronic Levels at Metal−Molecule Interfaces. *Phys. Rev. Lett.* **2006**, *97*, 216405.
49. Thygesen, K. S.; Rubio, A. Renormalization of Molecular Quasiparticle Levels at Metal−Molecule Interfaces: Trends across Binding Regimes. *Phys. Rev. Lett.* **2009**, *102*, 046802.
50. Liang, L.; Meunier, V. Electronic Structure of Assembled Graphene Nanoribbons: Substrate and Many-Body Effects. *Phys. Rev. B* **2012**, *86*, 195404.
51. Tamblyn, I.; Darancet, P.; Quek, S. Y.; Bonev, S. A.; Neaton, J. B. Electronic Energy Level Alignment at Metal−Molecule Interfaces with a GW Approach. *Phys. Rev. B* **2011**, *84*, 201402.